

Article

Not peer-reviewed version

---

# Assessment of Anesthetic Depth Through EEG Mode Decomposition Using Singular Spectrum Analysis

---

[Haruka Kida](#), [Tomomi Yamada](#), [Shoko Yamochi](#), Yurie Obata, [Fumimasa Amaya](#), [Teiji Sawa](#)\*

Posted Date: 1 January 2026

doi: 10.20944/preprints202601.0015.v1

Keywords: electroencephalogram; general anesthesia; depth of anesthesia; Hilbert–Huang transform; singular value decomposition; singular spectrum analysis



Preprints.org is a free multidisciplinary platform providing preprint service that is dedicated to making early versions of research outputs permanently available and citable. Preprints posted at Preprints.org appear in Web of Science, Crossref, Google Scholar, Scilit, Europe PMC.

Copyright: This open access article is published under a [Creative Commons CC BY 4.0 license](#), which permit the free download, distribution, and reuse, provided that the author and preprint are cited in any reuse.

Disclaimer/Publisher's Note: The statements, opinions, and data contained in all publications are solely those of the individual author(s) and contributor(s) and not of MDPI and/or the editor(s). MDPI and/or the editor(s) disclaim responsibility for any injury to people or property resulting from any ideas, methods, instructions, or products referred to in the content.

Article

# Assessment of Anesthetic Depth Through EEG Mode Decomposition Using Singular Spectrum Analysis

Haruka Kida <sup>1</sup>, Tomomi Yamada <sup>2</sup>, Shoko Yamochi <sup>2</sup>, Yurie Obata <sup>3</sup>, Fumimasa Amaya <sup>1</sup>  
and Teiji Sawa <sup>4,\*</sup>

<sup>1</sup> Department of Anesthesia, Fukuchiyama City Hospital, Kyoto 620-0056, and Department of Anesthesiology, Graduate School of Medical Science, North Medical Center, Kyoto Prefectural University of Medicine, Kyoto 629-2261, Japan

<sup>2</sup> Department of Anesthesiology, Graduate School of Medical Science, Kyoto Prefectural University of Medicine, Kyoto 602-8566, Japan

<sup>3</sup> Department of Anesthesiology, Yodogawa Christian Hospital, Yodogawa Christian Hospital, Osaka 533-0024, Japan

<sup>4</sup> Hospital of Kyoto Prefectural University of Medicine, Kyoto 602-8566, Japan

\* Correspondence: anesth@koto.kpu-m.ac.jp; Tel.: +81-75-251-5230

## Highlights

### What are the main findings?

- Singular spectrum analysis (SSA) combined with Hilbert transform enabled robust, high-resolution decomposition of non-stationary EEG signals during sevoflurane general anesthesia, effectively separating trends, rhythmic components, and fast activity without predefined frequency bands.
- SSA-derived intrinsic mode function (IMF) parameters showed strong correlations with the BIS, and multiple linear regression models using selected IMF center frequencies and total power accurately predicted BIS values during the transition from maintenance to emergence ( $R^2 \approx 0.88$ ).

### What are the implications of the main findings?

- SSA offers a physiologically grounded and temporally precise alternative to conventional Fourier-based EEG analysis for depth-of-anesthesia monitoring, overcoming limitations related to non-stationarity and fixed frequency assumptions.
- This approach has the potential to improve real-time, individualized anesthesia management and provides a scalable framework that could be integrated with advanced modeling or AI techniques to enhance patient safety and reduce the risk of over- or under-anesthesia.

## Abstract

(1) Background: Electroencephalography (EEG) is widely used to monitor the depth of anesthesia; however, conventional Fourier-based analyses are limited in their ability to characterize non-stationary anesthetic-induced EEG dynamics. In this study, we investigated the utility of singular spectrum analysis (SSA) combined with the Hilbert transform for extracting physiologically meaningful EEG features during sevoflurane general anesthesia. (2) Methods: Frontal EEG data from ten patients undergoing sevoflurane anesthesia were analyzed from the maintenance phase through emergence. Using SSA, short EEG segments were decomposed into six intrinsic mode functions (IMFs) without pre-specified basis functions or frequency bands. Hilbert spectral analysis was applied to each IMF to obtain instantaneous frequency and amplitude characteristics. (3) Results: The SSA-based decomposition clearly captured phase-dependent EEG changes, including  $\alpha$  spindle activity during maintenance and increasing high-frequency components preceding emergence. Multiple linear regression models incorporating IMF center frequencies and total power demonstrated strong correlations with the bispectral index (BIS), achieving high predictive accuracy ( $R^2 = 0.88$ , MAE < 4). Compared with conventional spectral approaches, SSA provided superior temporal resolution and stable feature extraction for non-stationary EEG signals. (4) Conclusions:

These findings indicate that SSA combined with Hilbert analysis is a robust framework for quantitative EEG analysis during general anesthesia and may enhance real-time, individualized assessments of anesthetic depth.

**Keywords:** electroencephalogram; general anesthesia; depth of anesthesia, Hilbert–Huang transform; singular value decomposition; singular spectrum analysis

---

## 1. Introduction

In patients under general anesthesia (GA), electroencephalography (EEG) results change significantly due to the hypnotic effects of anesthetic drugs, causing these patients to transition from an awake state to a state of unconsciousness [3–6]. As a result, monitoring and quantifying these changes in EEG results has facilitated the development of technologies to assess the depth of anesthesia, aiding in its management [7–9]. Since the late 1990s, commercial devices such as the bispectral index (BIS) monitor (Medtronic, Dublin, Ireland) and SEDLine (Masimo, Irvine, USA), which enable spectral analysis of EEG results, have become available. These devices use fast Fourier transform technology to detect changes in the frequency components of EEG results, calculate parameters related to the depth of anesthesia, and visualize the hypnotic effects of general anesthetics through changes in the power spectrum presented as density spectral array color maps. However, techniques that analyze changes in the frequency components of electroencephalographic signals during general anesthesia and translate them into quantitative assessments of anesthetic depth are still not fully established, as they are influenced by variables such as the type of anesthetic agent and patient age, and thus remain an area with considerable potential for further development.

While the Fourier transform is a powerful tool for analyzing stationary signals, it falls short for non-stationary signals. In such cases, the discrete wavelet transform is often used. This method, like the Fourier transform, decomposes data based on a basis set and is used in multi-resolution analysis [10]. However, with wavelet transforms, the time and frequency resolution changes depending on the scale of the basis function, and it is necessary to appropriately choose the type of wavelet and parameters (such as the number of scales and the range of analysis); this often requires experience and extensive trial and error, making this a significant drawback in EEG analysis.

Recently, techniques combining modal decomposition and the Hilbert transform have been investigated as new alternatives to the fast Fourier transform. EEG is considered to show the collection of micro-electrical activities of neuronal groups in the cerebral cortex. Mode decomposition methods appropriately decompose these electrical activities, capturing them as the activity of virtual functional groups of cells and observing their modes. On the other hand, the Hilbert transform is a signal processing technique in the complex domain that shifts the phase by 90 degrees to obtain the instantaneous amplitude (IA) and frequency (IF). The Hilbert–Huang Transform, which combines empirical mode decomposition (EMD) with the Hilbert transform, has been reported to be effective for analyzing non-stationary time series and impulse data [11]. We have also published research in which we applied the Hilbert–Huang Transform to EEGs during propofol-induced GA [2]. Furthermore, we have evaluated the usefulness of various modal decomposition methods for EEG analysis during sevoflurane total anesthesia, including variational mode decomposition (VMD) [2,12], which decomposes EEGs into narrow-band mode functions, and the empirical wavelet transform (EWT), which uses Meyer wavelets to decompose into narrow frequency bands and assess them as precise band-pass filters for EEG decomposition [13,14].

In this study, we introduce a novel method for mode decomposition of time series data using singular spectrum analysis (SSA) [15,16]. This method is particularly suitable for non-stationary signals and does not require the pre-specification of bases. SSA involves transforming one-dimensional time series data into a matrix via a one-to-one mapping, then applying singular value decomposition (SVD) to the matrix [17]. SSA extends the spectral decomposition, which involves eigenvalues and eigenspectra of Hermitian matrices in linear algebra, to arbitrary rectangular

matrices. It involves the use of SVD to extract trends, periodic components, and noise from data, such as time series, demonstrating its strength in analyzing non-stationary signals. In this research, we combine modal decomposition via SSA with the Hilbert transform for frequency analysis to investigate its utility for extracting EEG characteristics during GA with inhalational sevoflurane.

## 2. Theoretical background, methods, and materials

### 2.1. Algorithm for SVD

#### 2.1.1. Singular values, singular vectors, and SVD of a rectangular matrix

Let  $\mathbf{M}$  be a matrix over  $\mathbf{K}^{m \times n}$ . The adjoint matrix of  $\mathbf{M}$  is denoted by  $\mathbf{M}^*$ . For a matrix  $\mathbf{M}$  of size  $m \times n$  with complex numbers as its elements,  $\mathbf{M}^*$  is the  $n \times m$  matrix obtained by transposing  $\mathbf{M}$  and taking the complex conjugate of its elements. If  $\mathbf{M}$  consists entirely of real numbers, finding the adjoint of  $\mathbf{M}$  is equivalent to finding its transpose.

When there exists a pair of unit vectors  $\mathbf{u}$  in  $\mathbf{K}^m$  and  $\mathbf{v}$  in  $\mathbf{K}^n$  that satisfy the conditions

$$\mathbf{M}\mathbf{v} = \sigma\mathbf{u} \text{ and } \mathbf{M}^*\mathbf{u} = \sigma\mathbf{v} \quad (1)$$

for some non-negative real number  $\sigma$ , this real number  $\sigma$  is called the singular value of matrix  $\mathbf{M}$  (corresponding to vectors  $\mathbf{u}$  and  $\mathbf{v}$ ). Furthermore, vectors  $\mathbf{u}$  and  $\mathbf{v}$  are called the left singular vector and right singular vector of  $\mathbf{M}$ , respectively.

In the decomposition

$$\mathbf{M} = \mathbf{U}\mathbf{\Sigma}\mathbf{V}^* \quad (2)$$

the diagonal components of  $\mathbf{\Sigma}$  are equal to the singular values of  $\mathbf{M}$ , and the column vectors of the unitary matrices  $\mathbf{U}$  and  $\mathbf{V}$  consist of the left singular vectors and right singular vectors of matrix  $\mathbf{M}$ , respectively. Here, a unitary matrix is defined as a complex square matrix  $\mathbf{U}$  that satisfies

$$\mathbf{U}^*\mathbf{U} = \mathbf{U}\mathbf{U}^* = \mathbf{I} \quad (3)$$

where  $\mathbf{I}$  is the identity matrix, and  $\mathbf{U}^*$  is the adjoint matrix of  $\mathbf{U}$  ( $\mathbf{U}^* = \mathbf{U}^T$  for real matrices).

Thus, for real matrices, the adjoint is simply the transpose, and the real unitary matrices are equivalent to orthogonal matrices. When extended to the complex number field, these become unitary matrices. Accordingly, an  $m \times n$  matrix  $\mathbf{M}$  has at least one and at most  $d = \min(m, n)$  distinct singular values. There always exists a unitary basis in  $\mathbf{K}^m$  consisting of the left singular vectors of  $\mathbf{M}$ , and there always exists a unitary basis in  $\mathbf{K}^n$  consisting of the right singular vectors of  $\mathbf{M}$ .

#### 2.1.2. SVD of EEG

Consider the time series of EEG voltage (in microvolts) sampled at 128 Hz for 3 seconds ( $N + 1 = 384$ ), denoted by

$$\mathbf{F} = \{x_0, x_1, x_2, \dots, x_{N-1}\} \quad (4)$$

To apply SSA to the EEG time series data, first, set the window length to  $K = 256$  (corresponding to 2 seconds of data) and extract 128 columns ( $L = 128$ ) of time series data by sliding the window. Then, construct a matrix known as a Hankel matrix in the following form:

$$\mathbf{X} = \begin{pmatrix} x_0 & x_1 & \cdots & x_{K-1} \\ x_1 & x_2 & \vdots & x_K \\ \vdots & \vdots & \ddots & \vdots \\ x_{L-1} & x_L & \cdots & x_{N-1} \end{pmatrix} \quad (5)$$

The first row consists of  $K$  data points from  $x_0$  to  $x_{K-1}$ , the second row consists of  $K$  data points from  $x_1$  to  $x_K$ , the third row consists of  $K = 256$  data points from  $x_2$  to  $x_{K+1}$ , and so on, until the right end of the sliding window reaches the last data point of the EEG time series,  $x_{N-1}$ . This process is repeated 128 times ( $L = N - K + 1$ ,  $128 = 383 - 256 + 1$ ). In the trajectory matrix, the same components appear from the top right to the bottom left, which is a characteristic of a Hankel matrix. The columns of  $\mathbf{X}$  are called  $L$ -lagged vectors, and the rows are called  $K$ -lagged vectors.

In the second step, the trajectory matrix is decomposed using SVD.

$$\mathbf{X} = \mathbf{U}\mathbf{\Sigma}\mathbf{V}^T \quad (6)$$

Here,  $\mathbf{U}$  is an  $L \times L$  unitary matrix (i.e.,  $\mathbf{U}\mathbf{U}^* = \mathbf{I}$ ) containing an orthonormal set of left singular vectors of  $\mathbf{X}$ .  $\mathbf{\Sigma}$  is an  $L \times K$  rectangular diagonal matrix that contains the  $d$  (where  $d = \min(K, L)$ ) singular values of  $\mathbf{X}$  in descending order.  $\mathbf{V}$  is a  $K \times K$  unitary matrix containing an orthonormal set of right singular vectors of  $\mathbf{X}$ .

Since  $\mathbf{\Sigma}$  has nonzero entries only on its diagonal, the matrix product  $\mathbf{U}\mathbf{\Sigma}\mathbf{V}^T$  can be expanded as a sum of rank-one matrices. Then,  $\mathbf{X}$  can be decomposed as

$$\mathbf{X} = \sigma_0 \mathbf{u}_0 \mathbf{v}_0^T + \sigma_1 \mathbf{u}_1 \mathbf{v}_1^T + \dots + \sigma_{d-1} \mathbf{u}_{d-1} \mathbf{v}_{d-1}^T \quad (7)$$

In this decomposition, the weights corresponding to the singular values determine the contribution of each basis, and the magnitude of the singular values indicates the relative importance of each basis. Equivalently, using summation notation, this decomposition can be expressed as follows:

$$\mathbf{X} = \sum_{i=0}^{d-1} \sigma_i \mathbf{u}_i \mathbf{v}_i^T \equiv \sum_{i=0}^{d-1} \mathbf{X}_i \quad (8)$$

Here, the parameter  $d (\leq L)$  is the rank of the trajectory matrix,  $\sigma_i$  denotes the  $i$ -th singular value of  $\mathbf{X}$ , and  $\mathbf{u}_i$  and  $\mathbf{v}_i$  are the corresponding left and right singular vectors, given by the  $i$ -th columns of  $\mathbf{U}$  and  $\mathbf{V}$ , respectively. The set  $\{\mathbf{u}_i, \sigma_i, \mathbf{v}_i\}$  is called the  $i$ -th eigentriple of the SVD. In this way, applying SVD to the trajectory matrix decomposes it into  $d$  matrices  $\mathbf{X}_i = \sigma_i \mathbf{u}_i \mathbf{v}_i^T$ , where the significant components have larger singular values  $\sigma_i$ .

In the case of dimensionality reduction, only the components that need to be retained are kept and used for reconstruction. For example, in noise reduction, one can look at the singular values and retain only those above a certain threshold. In the case of EEG analysis, grouping all components into several categories can be used for feature extraction.

### 2.1.3. Time series component separation and grouping

Up to this point, the EEG time series  $\mathbf{F}$  has been embedded into a sequence of  $L$ -lagged vectors, thereby forming the trajectory matrix of  $\mathbf{F}$ . SVD is then applied to this matrix, resulting in a set of elementary matrices whose sum reconstructs the original trajectory matrix. In an ideal scenario, the time series  $\mathbf{F}$  can be decomposed into a sum of mutually separable components,  $\mathbf{F} = \sum_j \mathbf{F}^{(j)}$ . By appropriately grouping the corresponding elementary matrices  $\mathbf{X}_i$ , the trajectory matrix can be expressed as

$$\mathbf{X} = \sum_{k \in S} \mathbf{X}_k + \sum_{l \in T} \mathbf{X}_l + \dots = \sum_j \mathbf{X}^{(j)} \quad (9)$$

where  $S$  and  $T$  are mutually exclusive index sets, and  $\mathbf{X}^{(j)}$  represents the trajectory matrix corresponding to the component  $\mathbf{F}^{(j)}$ . Each  $\mathbf{X}^{(j)}$  preserves the Hankel structure of the original trajectory matrix. The reconstructed time series  $\mathbf{F}^{(j)}$  is then obtained via diagonal averaging, in which the elements of  $\mathbf{X}^{(j)}$  are averaged along anti-diagonals extending from the upper right to the lower left of the matrix.

The element  $\tilde{\mathbf{x}}_{(p,q)}$  of the reconstructed matrix  $\tilde{\mathbf{X}}^{(j)}$ , with  $s = p + q$ ,  $K = 256 \geq L = 128$ , and  $s = 0, 1, \dots, N - 1$ , is defined by the diagonal averaging operation as follows:

$$\mathbf{F}_s^{(j)} \equiv \tilde{\mathbf{x}}_{(p,q)} = \begin{cases} \frac{1}{s+1} \sum_{p=0}^s \tilde{\mathbf{x}}^{(j)}_{(p, s-p)} & (0 \leq s \leq L-2) \\ \frac{1}{L} \sum_{p=0}^{L-1} \tilde{\mathbf{x}}^{(j)}_{(p, s-p)} & (L-2 \leq s \leq K-1) \\ \frac{1}{L+K-s-1} \sum_{p=s-K+1}^{L-1} \tilde{\mathbf{x}}^{(j)}_{(p, s-p)} & (K \leq s \leq K+L-2) \end{cases} \quad (10)$$

Each grouped time series, obtained by summing selected elementary components, is treated as an intrinsic mode function (IMF), to which the Hilbert transform is applied.

### 2.1.4. Computer Programming for SVD

A sample program for matrix calculations for SVD is provided in **Appendix A**. The Python program code for SVD is shown in **Table A1 (Additional file 1)**, and the Java program code is shown in **Table A2 (Additional file 2)**.

### 2.1.5. Hilbert transform

The Hilbert transform is applied to the IMF components, denoted by  $imf(t)$ , and the analytic signal  $z(t)$  is obtained as follows [1,2,11,18–21]:

$$\text{Analytic signal } z(t) = imf(t) + iH[imf(t)] = a(t)e^{i \int \omega(t) dt} \quad (11)$$

$$\text{in which } a(t) = \sqrt{imf(t)^2 + H[imf(t)]^2} \quad \text{Instantaneous amplitude (IA)} \quad (12)$$

$$\omega(t) = \frac{t}{dt} \left[ \tan^{-1} \left( \frac{H[imf(t)]}{imf(t)} \right) \right] \quad \text{Instantaneous frequency (IF)} \quad (13)$$

$$h(\omega) = \int H(\omega, t) dt \quad \text{Marginal Hilbert spectrum} \quad (14)$$

where  $\omega(t)$  and  $a(t)$  are the IF and the IA of the IMF used to obtain a time–frequency distribution for signal  $imf(t)$  and the Hilbert amplitude spectrum  $H(\omega, t)$ .

### 2.3. Anesthesia Management and Data Acquisition

This study used a previously reported [2] and publicly available dataset of EEG data from patients under sevoflurane GA (ten minutes until awakening in ten cases of GA, [https://github.com/teijisw/EEG\\_DataSet/tree/master/general\\_anesth\\_sevoflurane](https://github.com/teijisw/EEG_DataSet/tree/master/general_anesth_sevoflurane)) (**Additional File 3**). The original data acquisition was performed using EEG Analyzer software [22] (EEG Analyzer ver. 54\_GP, [http://anesth-kpum.org/blog\\_ts/?p=3169](http://anesth-kpum.org/blog_ts/?p=3169)) linked to a VISTA A-3000 BIS monitor with a BIS Quatro sensor [22]. For more details on patient information, anesthesia management, and data acquisition, such as the raw EEG, BIS, 95% spectral edge frequency (SEF<sub>95</sub>), total power (TP), and absolute power derived from electromyography in the 70–110 Hz range (EMG<sub>low</sub>), please refer to our previous report [2].

### 2.4. Data Processing and Statistics

The changes in the various EEG parameters between two time points were compared statistically by conducting Kruskal–Wallis tests with SPSS Statistics (28.0.1.0, IBM Corp., Armonk, NY, USA), and  $p$ -values  $< 0.05$  were considered statistically significant. Multiple linear regression (MLR) analysis of the BIS and IMF parameters was performed using the scikit-learn [17] and StatsModels libraries in Python (ver. 3.8), as in our recent reports [23,24].

## 3. Results

Using an EEG dataset from 10 cases of general anesthesia with sevoflurane, mode decomposition was performed using SAA. This dataset consisted of single-channel frontal EEG recordings from a BIS monitor, spanning 10 minutes from the maintenance phase of general anesthesia to the emergence phase.

### 3.1. Case Analysis of SSA Application

First, we present the SAA that was conducted using the EEG data acquired from Patient #1 (a 54-year-old female who was diagnosed with IgA nephropathy and underwent palatine tonsillectomy) [2] anesthetized with sevoflurane. We analyzed 3 s long epochs of EEG data that were recorded at 128 Hz during three distinct phases of GA up to the point of emergence: the maintenance (10 min before emergence), transition (1 min before emergence), and emergence phases. From each 3-second segment containing 384 data points, a trajectory matrix of 128 rows  $\times$  256 columns was constructed using a 2-second window (256 data points), shifted by 1 data point at a time. Then, a

process was applied to group the elementary matrices into several component sets and subsequently reconstruct each set into a time series (**Figure 1**).

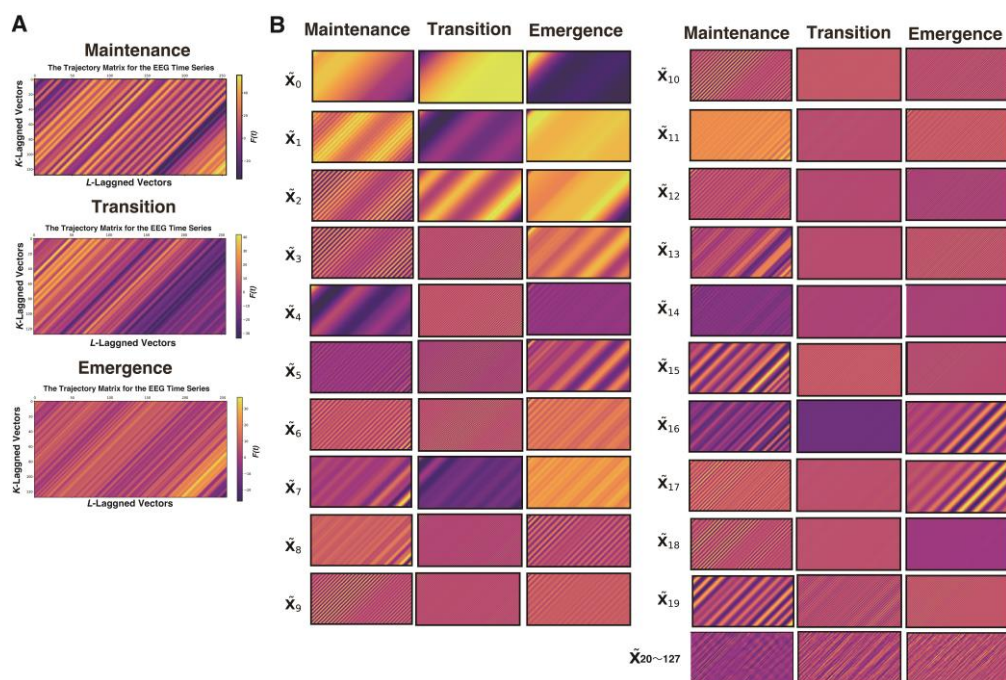


**Figure 1.** An inspection of 128 trajectory matrices of EEG time series across three phases of sevoflurane general anesthesia: **A)** color maps of the Hankelized trajectory matrices of EEG time series before SSA decomposition, and **B)** an inspection of the first 20 and the remaining 108 elementary matrices after SSA decomposition, across the three phases of sevoflurane general anesthesia.

A process was applied to convert each elementary matrix into a Hankel matrix and subsequently reconstruct it into a time series. The color visualization of the trajectory matrix of the EEG time series highlights the characteristics of the elementary matrices. For example,  $\tilde{X}_0$  and  $\tilde{X}_1$  changed very gradually throughout the entire time series and can be interpreted as trend components.  $\tilde{X}_2$  and  $\tilde{X}_3$  also often exhibited slow periodicity. In the range from approximately  $\tilde{X}_4$  to  $\tilde{X}_9$ , periodicity was frequently visible, whereas from  $\tilde{X}_{10}$  onward, the components consisted of fine waves with high frequencies.

The relative contributions

$$\frac{\sigma_i^2}{\sum_{k=0}^{d-1} \sigma_k^2} \quad (15)$$

and cumulative contributions

$$\frac{\sum_{j=0}^i \sigma_j^2}{\sum_{k=0}^{d-1} \sigma_k^2} \quad (16)$$

of the first 64 elementary matrices  $X_i$  in the decomposition  $X = \sum_{i=0}^{d-1} X_i$  obtained via SVD of 3-second EEG segments in the three phases of general anesthesia (**Figure 2**). The elementary matrices  $X_0$  and  $X_1$  contributed 22% and 21%, respectively, to the overall decomposition of  $X$ . The first 20 elementary matrices together accounted for 97% of the total contribution. In this study, the 128 matrices obtained via SAA were grouped into six sets: 0–1, 2–3, 4–6, 7–9, 10–19, and 20–127. The matrices within each group were summed:

$$\tilde{X}_0 \sim \tilde{X}_1, \tilde{X}_2 \sim \tilde{X}_3, \tilde{X}_4 \sim \tilde{X}_6, \tilde{X}_7 \sim \tilde{X}_9, \tilde{X}_{10} \sim \tilde{X}_{19}, \tilde{X}_{20} \sim \tilde{X}_{127} \quad (17)$$

$$\tilde{X}^{(\text{IMF-1})} = \tilde{X}_0 + \tilde{X}_1 \Rightarrow \tilde{F}^{(\text{IMF-1})} = \tilde{F}_0 + \tilde{F}_1 \quad (18)$$

$$\tilde{X}^{(\text{IMF-2})} = \tilde{X}_2 + \tilde{X}_3 \Rightarrow \tilde{F}^{(\text{IMF-2})} = \tilde{F}_2 + \tilde{F}_3 \quad (19)$$

$$\tilde{X}^{(\text{IMF-3})} = \tilde{X}_4 + \tilde{X}_5 + \tilde{X}_6 \Rightarrow \tilde{F}^{(\text{IMF-3})} = \tilde{F}_4 + \tilde{F}_5 + \tilde{F}_6 \quad (20)$$

$$\tilde{X}^{(\text{IMF-4})} = \tilde{X}_7 + \tilde{X}_8 + \tilde{X}_9 \Rightarrow \tilde{F}^{(\text{IMF-4})} = \tilde{F}_7 + \tilde{F}_8 + \tilde{F}_9 \quad (21)$$

$$\tilde{X}^{(\text{IMF-5})} = \tilde{X}_{10} + \dots + \tilde{X}_{19} \Rightarrow \tilde{F}^{(\text{IMF-5})} = \tilde{F}_{10} + \dots + \tilde{F}_{19} \quad (22)$$

$$\tilde{X}^{(\text{IMF-6})} = \tilde{X}_{20} + \dots + \tilde{X}_{127} \Rightarrow \tilde{F}^{(\text{IMF-6})} = \tilde{F}_{20} + \dots + \tilde{F}_{127} \quad (23)$$

where  $\tilde{F}^{(\text{IMF-}i)}$  is an IMF time series.

Using SAA, each 3-second EEG signal was decomposed into six intrinsic mode functions (IMFs) according to the above classification. According to the rules of mode decomposition, the original EEG waveform can be reconstructed by aligning the time axes and summing the voltage values of the six IMFs. The Hilbert transform was then applied to each IMF to obtain the Hilbert spectrum.

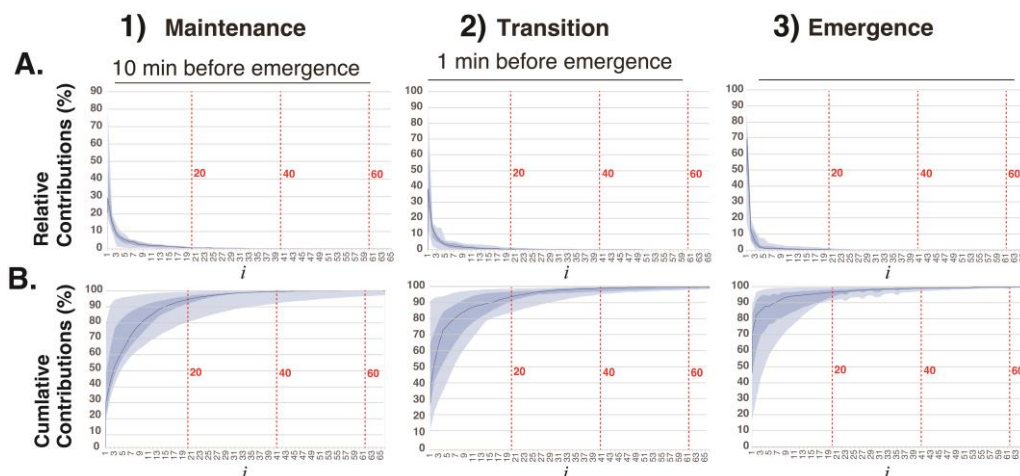


**Figure 2.** Plots of the A) relative and B) cumulative contributions of the 64 elementary matrices to the trajectory matrix of the EEG time series in three phases (1: maintenance, 10 min before emergence; 2: transition, 1 min before emergence; 3: emergence) of sevoflurane general anesthesia.

**Figure 3** presents the raw EEG data (3 s), density spectral arrays (DSAs) (64 s, starting with a 3 s long segment of raw EEG data), trajectory matrix images of EEG time series, IMFs obtained over 3 s via the SSA method, and Hilbert spectrograms across these GA phases for Patient #1 (54-year-old woman, Yamada et al., 2023 [2]). During the maintenance phase of anesthesia, IMFs 1-4 were predominantly in the frequency range of around 15 Hz or lower. In the DSA during the maintenance phase, an enhancement of  $\alpha$  waves characteristic of sevoflurane general anesthesia was observed, with increased power around 12 Hz. Correspondingly, spindle waves, indicative of  $\alpha$  wave

enhancement, were visible in the EEG waveform. In the DSA during the transitional phase, while the  $\alpha$  enhancement persisted, there was an additional increase in higher-frequency components between 15 and 47 Hz. Compared to that for the maintenance phase, the EEG waveform showed reduced amplitude and the emergence of fast-frequency components.

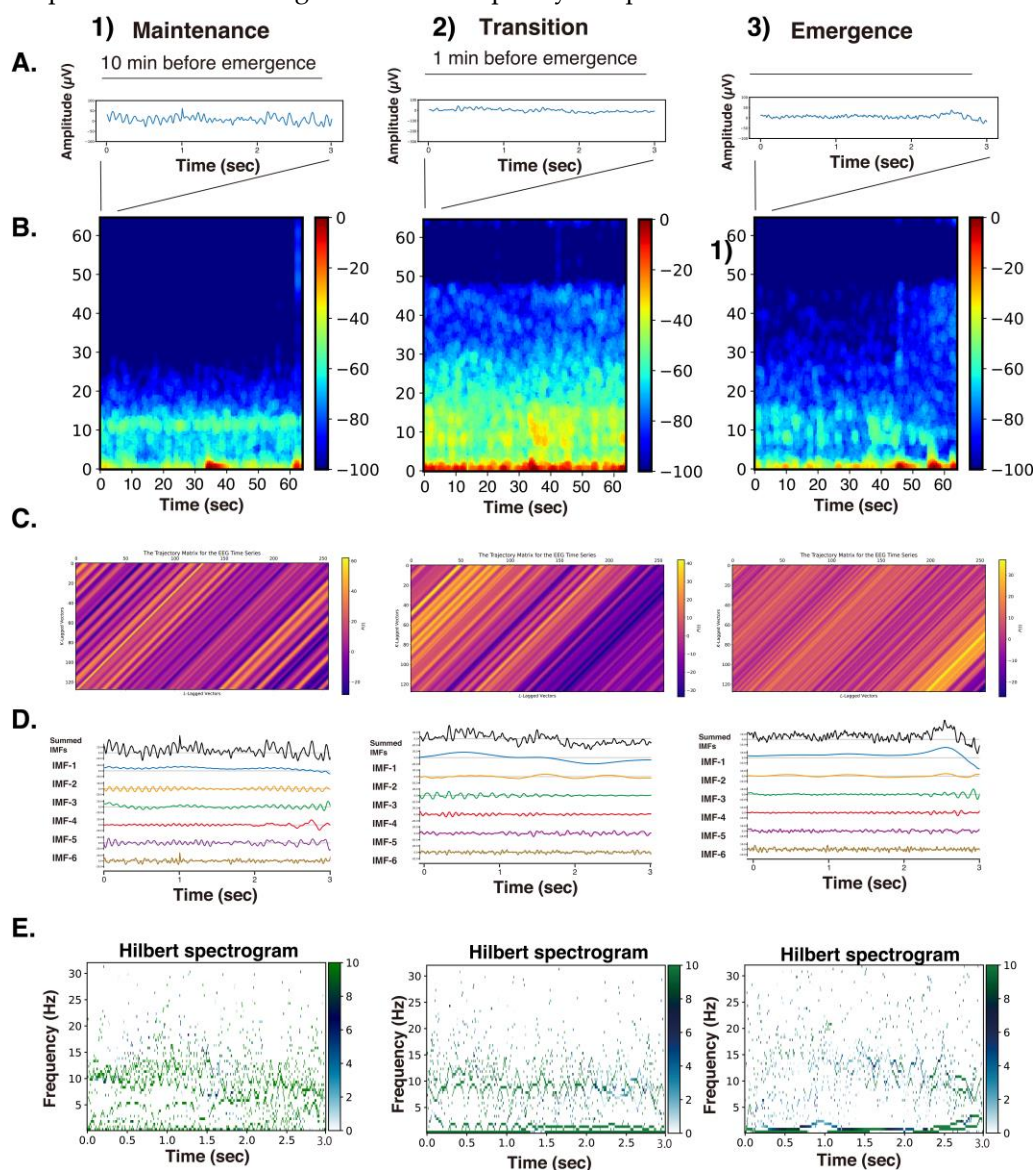


**Figure 3.** A) The raw EEG data (3 s), B) density spectral arrays (DSAs) (64 s, starting with a 3 s long segment of raw EEG data), C) trajectory matrix images of EEG time series, D) IMFs obtained over 3 s via SSA methods, and E) Hilbert spectrograms across three GA phases (1: maintenance, 10 min before emergence; 2: transition, 1 min before emergence; 3: emergence) in Patient #1 (54-year-old woman, Yamada et al., 2023 [2]).

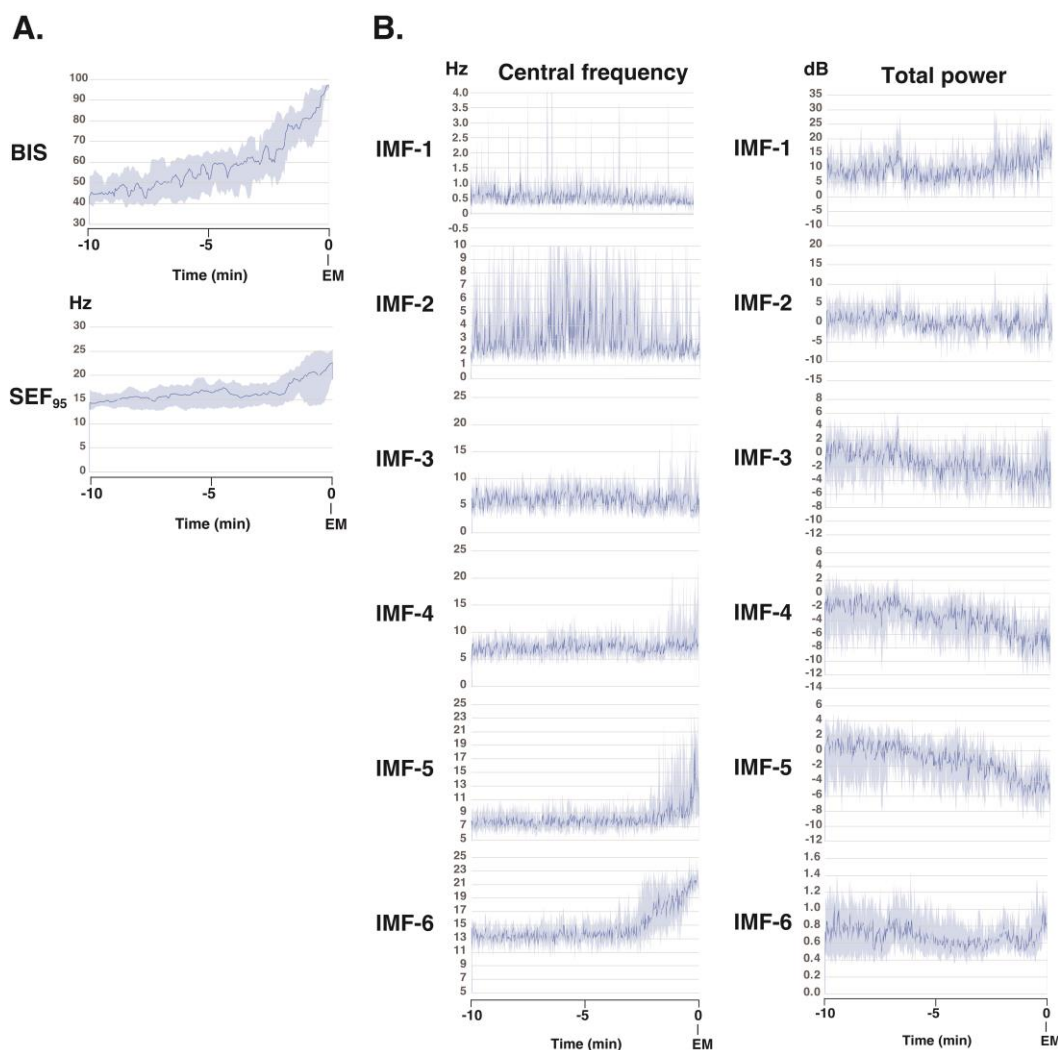


**Figure 4.** Time course changes in the **A)** processed EEG parameters (BIS index, SEF<sub>95</sub>), **B)** central frequencies, and **C)** total powers of the intrinsic mode functions (IMFs) of the singular value decomposition (SVD) for 10 min before emergence from general anesthesia in ten patients[1]. The total power is displayed on a log scale (in decibels (dB)); obtained from the power ( $P$ ,  $\mu\text{V}^2$ ) using the conversion  $\text{dB} = 10 \times \log_{10}P$ ). The data are presented as medians (dark blue lines), and 25th–75th percentile ranges (light blue areas). BIS index: bispectral index, SEF<sub>95</sub>: spectral edge frequency 95%, EM: emergence.

In the awakening phase, the  $\alpha$  wave enhancement disappeared, and although the fast-frequency components persisted, an overall reduction in power was observed. The EEG waveform during this phase was predominantly composed of low-amplitude  $\beta$  wave activity. When the trajectory matrices were compared across the three phases, the maintenance and transitional phases exhibited coarser diagonal striations indicative of periodicity, whereas the awakening phase showed finer diagonal patterns. The middle panels of **Figure 3** display the six IMFs of the EEG signals, obtained through SAA. In the maintenance phase, IMF-2 and IMF-3 captured the spindle waves associated with enhanced  $\alpha$  activity. In the transitional phase, the spindle wave in IMF-2 disappeared. In the awakening phase, IMF-1 through IMF-3 presented nearly flat waveforms, while IMF-5 and IMF-6 predominantly exhibited fast wave activity. The bottom panels of **Figure 3** show the Hilbert spectrograms for each IMF over a 3-second interval, depicting the time series relationship between IA and IF obtained via Hilbert transform. In the maintenance phase, a characteristic band around 10 Hz was evident. This feature was also present around 8–10 Hz during the transitional phase. However, in the awakening phase, these characteristic bands disappeared.

**Table 1.** Multiple linear regression analysis between the BIS values and parameters of the IMFs in the dynamic mode decomposition.

A. SSA with all 12 IMF parameters			
determination factor ( $R^2$ )		0.880	
MAE		3.625	
RMSE		4.525	
y-intercept		6.541	
explanatory variables		regression coefficient	$P >  t $
central frequency	IMF-1	-2.471442	0.034*
	IMF-2	0.516911	0.001*
	IMF-3	-0.150217	0.354
	IMF-4	0.268052	0.203
	IMF-5	1.140631	0.000*
	IMF-6	2.587983	0.000*
total power	IMF-1	0.226694	0.005*
	IMF-2	0.040186	0.773
	IMF-3	-0.394622	0.030*
	IMF-4	-0.600540	0.004*
	IMF-5	-1.753359	0.000*
	IMF-6	-5.112977	0.034*
B. SSA with 9 significant IMF parameters			
determination factor ( $R^2$ )		0.880	
MAE		3.636	
RMSE		4.534	
y-intercept		7.288	
explanatory variables		regression coefficient	$P >  t $
central frequency	IMF-1	-2.443025	0.001*
	IMF-2	0.478588	0.036*
	IMF-5	1.180527	0.002*
	IMF-6	2.583207	0.000*
total power	IMF-1	0.237894	0.000*
	IMF-3	-0.375238	0.002*
	IMF-4	-0.611259	0.029*
	IMF-5	-1.752437	0.003*
	IMF-6	-5.137877	0.033*

The objective variable was the median BIS value from the 10 patients, and the explanatory variables were the median central frequencies and total powers of the IMFs in the SSA. The explanatory variables were **A)** 12 IMF parameters or **B)** 9 significant explanatory parameters. The EEG data were obtained from the last 10 minutes before emergence in 10 patients who received sevoflurane general anesthesia. MAE: mean absolute error; RMSE: root-mean-squared error; SSA: singular spectrum analysis; \* $p < 0.05$ .

### 3.2. Hilbert Spectrograms of the IMFs in the SSA Method

To gain further understanding of the frequency characteristics of each IMF produced via SSA across the 10-minute phase before emergence, a Hilbert spectral analysis of the IMFs was performed. This analysis assessed variations in the IF and IA values derived from the Hilbert transforms of the IMFs across each phase for all 10 patients (**Figure 4**). Video images (**Additional files 4-13**) present the analysis screens (the Hilbert spectrograms for each IMF obtained via the SSA method, the summed IMF (IMF-all, which corresponds to the original EEG data), and the DSAs for 30 min until emergence) for the 30-minute period up to the awakening phase in these 10 cases. During the 10-minute period from the maintenance phase of general anesthesia to the awakening phase, the BIS value gradually increased from approximately 45 to 95. The SEF<sub>95</sub> began to rise two minutes prior to awakening, increasing from around 14 Hz to approximately 23 Hz at the time of awakening. Using SAA, the EEG was decomposed into six IMFs, and the changes in IF for each IMF were analyzed. IMF-1 showed a

mild, gradual decrease; IMF-2 exhibited significant variability; IMF-3 and -4 remained relatively stable; IMF-5 began to increase two minutes before awakening; and IMF-6 began to increase three minutes before awakening. Regarding the changes in IA of each IMF, IMF-1 showed a mild, gradual increase, while IMF-2 through -5 demonstrated a gradual decrease.

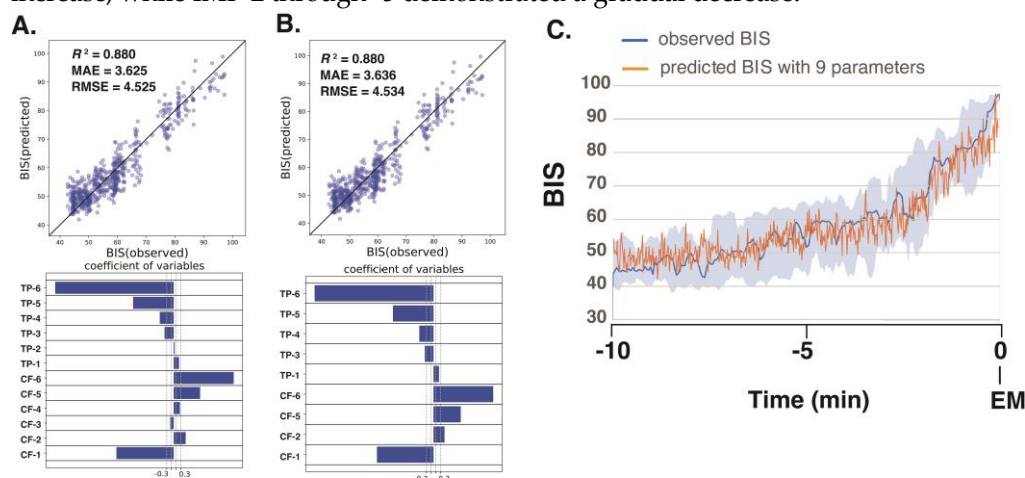


**Figure 5.** Multiple linear regression (MLR) analysis was performed with the BIS values from the BIS monitor as the objective variable and the statistically significant center frequency (CF) and total power (TP) medians of IMF-1 to IMF-5 obtained via SSA decomposition as explanatory variables for the 10 minutes before emergence in the ten patients [2]. **A.** MLR with all 12 parameters of IMFs. **B.** MLR with 9 significant parameters of IMFs. The correlation between the observed BIS and predicted BIS was calculated from the MLR and the coefficient variables. **C.** The time-course changes in the observed and predicted BIS derived from MLR using 9 parameters were computed from the MLR. The data are presented as medians (dark blue lines), 25th–75th percentile ranges (light blue areas), and predicted BIS values (orange line). BIS, bispectral index; EM, emergence; TP, total power; CF, central frequency of instantaneous frequency.  $R^2$ , coefficient of determination; MAE, mean absolute error; RMSE, root-mean-squared error.

### 3.4. Multiple Linear Regression Models to Predict the BIS

Next, we analyzed the processed EEG data, sampled every 8 s, acquired 10 min before emergence from 10 patients who had been administered sevoflurane GA. We explored the relationship between the BIS (a clinical gauge of the depth of anesthesia) and the IMF parameters, including the center frequency (i.e., the average of the Hilbert spectrum) and TP, which were converted from power in  $P(\mu V^2)$  to decibels (dB) using  $dB = 10 \cdot \log_{10} P$ . Multiple linear regression (MLR) models were developed using IMF parameters to predict the BIS using the Data\_EME10s dataset. The comprehensive MLR formula included individual terms for the center frequencies and the TPs of the six IMFs, yielding a model with 12 explanatory variables.

The analysis yielded robust correlations, with the SSA-based MLR model using all 12 parameters (6 center frequencies and 6 TPs) demonstrating the strongest correlation ( $R^2=0.880$ ) and the lowest errors (mean absolute error: MAE = 3.625; root-mean-squared error: RMSE = 4.525) among the four models examined; the results are detailed in **Table 1**. Notably, in the SAA approach, the center frequencies of IMF-1, IMF-2, IMF-5, and IMF-6 and the TPs of IMF-1, IMF-3, IMF-4, IMF-5, and IMF-6 were identified as significant predictors. For a more targeted approach, we evaluated an MLR model using only nine IMF parameters (IMF-1\_freq, IMF-2\_freq, IMF-5\_freq, IMF-6\_freq, IMF-1\_TP, IMF-3\_TP, IMF-4\_TP, IMF-5\_TP, and IMF-6\_TP) that presented significant  $p$ -values (less than 0.05), and the model still presented excellent fit metrics ( $R^2=0.880$ , MAE = 3.636, RMSE = 04.534) (**Figure 5**). This finding indicates that SAA effectively captures narrow-band changes in IMF parameters correlated with shifts in the BIS during emergence from GA, thereby demonstrating superior sensitivity for monitoring changes in the depth of anesthesia. The multiple linear regression equation derived from these nine significant parameters was used to predict BIS values over the 10-minute period leading up to awakening, and the predicted values accurately reflected the actual changes in the measured BIS values.

## 4. Discussion

Monitoring the depth of general anesthesia using EEG remains a complex challenge, largely due to variability in anesthetic agents and patient-specific factors such as age-related neurophysiological differences in pediatric and geriatric populations. Although EEG-based depth indices provided by commercially available monitors have proven useful [7] [9], they are primarily calibrated for intravenous agents like propofol and volatile anesthetics such as sevoflurane. This narrow optimization limits their generalizability to other anesthetic agents and patient groups. To improve depth-of-anesthesia monitoring, a more robust approach grounded in physiologically informed, scientifically validated algorithms is needed.

Quantitative analysis of these EEG spectral dynamics is essential for developing mathematical models that accurately capture the relationship between anesthetic pharmacodynamics and the depth of anesthesia. Such models could substantially enhance the precision and universality of depth-of-anesthesia assessments across diverse clinical scenarios. Frontal EEG signals recorded during GA exhibit characteristic changes in response to anesthetic-induced modulation of neurophysiological activity. Specifically, there is a marked suppression of higher-frequency  $\beta$  and  $\gamma$  activity—typically associated with alertness—while the power of slower-frequency components, such as  $\delta$  and  $\theta$  waves, increases, reflecting deeper hypnotic states [4–6]. Additionally, a pronounced rise in  $\alpha$  activity, often associated with sleep spindles, is observed as anesthesia deepens.

To more effectively extract such EEG features, our recent study examined the use of mode decomposition techniques—EMD, VMD, and EWT—combined with the Hilbert transform, which offers a higher temporal resolution than conventional Fourier-based approaches [2,14]. While both VMD and EWT effectively capture frequency dynamics, they exhibit inconsistencies in assigning narrow-band components across successive epochs, limiting their reliability for continuous depth-of-anesthesia assessment. On the other hand, wavelet mode decomposition (WMD), which we previously reported as an application of EWT, can stabilize the central frequency and TP of the IMFs by using predefined frequency bands [14]. This method demonstrated a strong correlation with BIS values, particularly during the critical 10-minute period from maintenance to emergence from anesthesia. Multiple regression analysis revealed that specific central frequencies and TP values of WMD-derived IMFs were significantly associated with changes in the depth of anesthesia. However, decomposing EEG signals into fixed frequency bands is conceptually equivalent to applying bandpass filters. Although this strategy is useful when the frequency bands of interest are well defined, it carries the inherent risk of missing characteristic changes that span multiple frequency bands, particularly when the relevant spectral features are not clearly established.

To address these limitations, we applied SSA for the first time to extract frequency features from EEG signals recorded during general anesthesia. EEG signals under general anesthesia exhibit time-varying, nonlinear, and non-stationary characteristics. SSA enables the decomposition of such complex signals while preserving their intrinsic statistical structure [25]. Unlike linear approaches such as the Fourier transform, SSA provides high-fidelity separation of trends, periodic components, and noise, making it a promising method for characterizing EEG dynamics under anesthesia. The elementary components derived from SSA capture distinct rhythmic activities such as  $\alpha$  (8–13 Hz) and  $\theta$  (4–7 Hz) waves, which are modulated by anesthetic agents. These components change in proportion to the depth of anesthesia and can be used to extract quantitative, phase-preserving indicators of anesthetic depth. Trajectory matrices and singular vectors obtained via SSA effectively visualize and quantify dynamic changes in EEG across the different anesthetic phases—maintenance, transition, and emergence. This approach offers potential as a real-time analytic framework for assessing state transitions under general anesthesia. EEG decomposition via SSA, when integrated with deep learning and state-space modeling, holds promise for advancing precision anesthesia—individualized anesthetic management tailored to patient-specific neurophysiological responses. Such innovations may enhance patient safety and reduce the risk of over-anesthesia.

In contrast to the Fourier transform, which decomposes signals into frequency components to generate spectrograms, the combined application of mode decomposition and the Hilbert transform

offers a more refined approach to feature extraction. This method enables the calculation of the IF and IA at each data point, producing high-resolution spectrograms that more accurately reflect the signal's dynamic characteristics. By comparison, Fourier-based power spectral analysis—for instance, using 0.25 Hz frequency bins for a 128 Hz EEG sampling rate—requires at least 512 data points (equivalent to 4 seconds of EEG) and only achieves a temporal resolution of 2 seconds under a 50% window overlap. In this context, decomposing EEG signals into narrow-band intrinsic mode functions (IMFs) significantly improves the temporal resolution and enhances the granularity of time–frequency representations. The resulting Hilbert spectrogram allows for more detailed and precise analysis of non-stationary EEG signals.

The limitations of this study are inherently linked to a fundamental and unresolved question: What precisely constitutes the depth of anesthesia? [26] Currently, commercially available monitors rely on indices such as the BIS and patient state index (PSi) as surrogate markers for anesthetic depth. However, the proprietary nature of the algorithms underlying these indices renders their validity difficult to verify through direct comparison. In this study, we examined the relationship between BIS values and parameters derived from the Hilbert spectra of IMFs obtained via mode decomposition. Although the algorithm used to calculate the BIS has not been fully disclosed, this study demonstrated the potential for capturing changes in the frequency components of EEG signals during general anesthesia using singular spectrum analysis, a linear-algebra-based approach, and to translate these findings into a technique for assessing the depth of anesthesia.

## 5. Conclusions

This study demonstrated that SSA combined with the Hilbert transform enables high-resolution, physiologically meaningful decomposition of EEG signals from patients under general anesthesia. SSA effectively extracted time-varying features associated with anesthetic depth transitions, offering superior temporal precision. Multiple regression models using SSA-derived features accurately predicted BIS values, highlighting SSA's potential for improving real-time anesthesia monitoring.

**Supplementary Materials:** The following supporting information can be downloaded at <https://www.mdpi.com/article/doi/s1>, **Additional file 1:** File01\_python\_code for SVD (pdf). The Jupyter Notebook file of Python (ver. 3.8) code for the SSA. **Additional file 2:** File02\_java\_processing\_code for SSA (text). **Additional file 3:** File03\_EEG\_data\_10cases\_EME10min.zip. Archive data file containing tab-separated values of the raw EEG data (microvolts) for 10 min before emergence from GA in ten patients. **Additional file 4-13:** A video file showing SSA analysis of EEG data for the 30 min leading up to emergence in patients #1-#10. File04\_Sev1\_SSA.mp, patient #1. File05\_Sev2\_SSA.mp4, patient #2. File06\_Sev3\_SSA.mp4, patient #3. File07\_Sev4\_SSA.mp4, patient #4. File08\_Sev5\_SSA.mp4, patient #5. File09\_Sev6\_SSA.mp4, patient #6. File10\_Sev7\_SSA.mp4, patient #7. File11\_Sev8\_SSA.mp4, patient #8. File12\_Sev9\_SSA.mp4, patient #9. File13\_Sev10\_SSA.mp4, patient #10.

**Author Contributions:** Conceptualization, T.S.; methodology, T.S.; software, T.S.; validation, H.K. T.Y., S.Y., and Y.O.; formal analysis, H.K. and T.S.; investigation, H.K. T.Y., and T.S.; data curation, H.K. T.S., and T.Y.; writing—original draft preparation, T.S.; writing—review and editing, H.K. and T.S.; supervision, F.A.; project administration, T.S.

**Funding:** We performed this study with the support of internal funding from the Department of Anesthesiology, Kyoto Prefectural University of Medicine.

**Institutional Review Board Statement:** The EEG data used for spectral analyses in this study were obtained from anesthetized patients with ethical approval (No. ERB-C-1074-2) from the Institutional Review Board for Human Experiments at the Kyoto Prefectural University of Medicine (IRB of KPUM).

**Informed Consent Statement:** For this noninterventional and noninvasive retrospective observational study including minors, the requirement for informed patient consent was waived by the IRB of KPUM; however, patients were provided with an opt-out option, of which they were notified in the preoperative anesthesia clinic.

**Data Availability Statement:** The EEG dataset used herein is available on the author's GitHub site ([https://github.com/tejjisw/EEG\\_DataSet](https://github.com/tejjisw/EEG_DataSet)) [13]. The programming codes used in the analysis in this paper are available as supplementary data.

**Acknowledgments:** We thank Edanz (<https://jp.edanz.com/ac>) for editing a draft of this manuscript.

**Conflicts of Interest:** The authors declare no conflicts of interest.

## Abbreviations

The following abbreviations are used in this manuscript:

BIS	bispectral index
DSA	density spectral arrays
EEG	electroencephalography
EMD	empirical mode decomposition
EMG <sub>low</sub>	absolute power derived from electromyography in the 70–110 Hz range
EWT	empirical wavelet transform
IMF	intrinsic mode function
IA	instantaneous amplitude
IF	instantaneous frequency
MLR	multiple linear regression
SEF <sub>95</sub>	95% spectral edge frequency
SSA	singular spectrum analysis
SVD	singular value decomposition
TP	total power
VMD	variational mode decomposition
WMD	wavelet mode decomposition

## Appendix A1

### *Appendix 1: Python Computer Programming for SVD*

**Table A1.** Example python programming for SVD (Additional file 1: File01\_python\_code for SVD, pdf).

```

import numpy as np
import matplotlib.pyplot as plt
from scipy import signal
X = np.array([[1, 2, 3], [4, 5, 6]])

print(X)
-----
[[1 2 3]
 [4 5 6]]
-----
U, S, VT = np.linalg.svd(X) #Singular value decomposition, where S is a vector containing the
singular values in descending order.
V = VT.T

Sigma = np.zeros(X.shape) #Prepare a float64 matrix Sigma of the same size as X.

for ss in range(0, S.shape[0]):
    Sigma[ss, ss] = S[ss] #Arrange the singular values in a diagonal matrix.

print(U)
-----
[[-0.3863177 -0.92236578]
 [-0.92236578  0.3863177 ]]
print(Sigma)
[[9.508032  0.         0.         ]
 [0.         0.77286964 0.         ]]
-----

print(V)
-----
[[-0.42866713  0.80596391  0.40824829]
 [-0.56630692  0.11238241 -0.81649658]
 [-0.7039467  -0.58119908  0.40824829]]
X_SVD = U@Sigma@V.T # Matrix multiplication can be written using the @ operator.
-----

print(X_SVD)
-----
[[1. 2. 3.]
 [4. 5. 6.]]
-----

```

This Python code demonstrates SVD and its use in reconstructing a matrix. First, the code imports numerical and scientific libraries and defines a simple  $2 \times 3$  matrix,  $X$ . The matrix is then decomposed using `np.linalg.svd`, which factorizes  $X$  into three components:

- $U$ : a matrix whose columns are the left singular vectors;
- $\Sigma$  ( $S$ ): a one-dimensional array containing the singular values in descending order;
- $V^T$ : the transpose of the matrix of right singular vectors.

Next, the code constructs a diagonal matrix  $\Sigma$  from the singular values so that its dimensions match those of the original matrix. Each singular value is placed on the diagonal of  $\Sigma$ .

The matrices  $U$ ,  $\Sigma$ , and  $V$  (obtained by transposing  $V^T$ ) are then printed to show the results of the decomposition.

Finally, the original matrix is reconstructed by means of matrix multiplication using the `@` operator:

$$X = U \Sigma V^T$$

The reconstructed matrix `X_SVD` is printed and matches the original matrix  $X$ , demonstrating that the SVD correctly represents the original data.

### Appendix 2: Java Processing Computer Programming for SVD

**Table A2.** Example Java Processing programming for SVD (**Additional file 2:** File02\_java\_processing\_code for SSA, text).

```

import org.ejml.simple.SimpleMatrix;
import org.ejml.interfaces.decomposition.SingularValueDecomposition;
import org.ejml.dense.row.factory.DecompositionFactory_DDRM;

double[][] X = {
    {1, 2, 3},
    {4, 5, 6}
};

SimpleMatrix X_m = new SimpleMatrix(X).transpose();
SingularValueDecomposition svd = DecompositionFactory_DDRM.svd(X_m.numRows(),
X_m.numCols(), true, true, false);
svd.decompose(X_m.getMatrix());

SimpleMatrix U = SimpleMatrix.wrap(svd.getU(null, false));
SimpleMatrix S = SimpleMatrix.wrap(svd.getW(null));
SimpleMatrix V = SimpleMatrix.wrap(svd.getV(null, false));

for (int i=0; i< U.numCols(); i++) {
    for (int j=0; j< U.numRows(); j++) {
        println("U", i, j, ":", U.get(i, j));
    }
}

-----
U 0 0 : 0.4286671335486263
U 0 1 : -0.8059639085892979
U 0 2 : 0.40824829046386346
U 1 0 : 0.5663069188480352
U 1 1 : -0.11238241409659376
U 1 2 : -0.816496580927726
U 2 0 : 0.7039467041474441
U 2 1 : 0.5811990803961103
U 2 2 : 0.40824829046386296
-----

for (int i=0; i< S.numCols(); i++) {
    for (int j=0; j< S.numRows(); j++) {
        println("S", i, j, ":", S.get(j, i));
    }
}

-----
S 0 0 : 9.508032000695724
S 0 1 : 0.0
S 0 2 : 0.0
S 1 0 : 0.0
S 1 1 : 0.7728696356734849
S 1 2 : 0.0
-----

for (int i=0; i< V.numCols(); i++) {
    for (int j=0; j< V.numRows(); j++) {
        println("V", i, j, ":", V.get(j, i));
    }
}

```

```

-----
V 0 0 : 0.3863177031186116
V 0 1 : 0.9223657800770585
V 1 0 : 0.9223657800770585
V 1 1 : -0.3863177031186116
-----

SimpleMatrix X_SVD = (U.mult(S)).mult(V.transpose());
for (int i=0; i< X_SVD.numCols(); i++) {
    for (int j=0; j< X_SVD.numRows(); j++) {
        println("X_SVD", i, j, ":", X_SVD.get(j, i));
    }
}
-----

X_SVD 0 0 : 1.0
X_SVD 0 1 : 2.0000000000000004
X_SVD 0 2 : 3.0000000000000001
X_SVD 1 0 : 4.0000000000000003
X_SVD 1 1 : 5.0000000000000002
X_SVD 1 2 : 6.0
-----

```

This code performs SVD of a small matrix using the EJML (Efficient Java Matrix Library). First, a  $2 \times 3$  matrix,  $X$ , is defined and then transposed to form  $X_m$  so that the decomposition is applied to a  $3 \times 2$  matrix. The EJML SVD factory creates an SVD object that computes the full  $U$ ,  $\Sigma$  ( $S$ ), and  $V$  matrices.

The `decompose()` method factorizes the matrix as

$$X_m = U \Sigma V^T$$

$U$  contains the left singular vectors (orthonormal basis in the column space).

- $\Sigma$  is a diagonal matrix containing the singular values, which represent the strength of each mode.
- $V$  contains the right singular vectors (orthonormal basis in the row space).

After decomposition, the code extracts  $U$ ,  $\Sigma$ , and  $V$  as SimpleMatrix objects and prints their elements using nested loops. The printed results show

- $U$  as a  $3 \times 3$  orthonormal matrix;
- $\Sigma$  with two non-zero singular values (reflecting the rank of the original matrix);
- $V$  as a  $2 \times 2$  orthonormal matrix.

Overall, this code demonstrates how to compute and inspect the components of the SVD in Java/Processing using EJML, a widely used library for dimensionality reduction, noise filtering, and modal decomposition.

## References

1. Yamada, T.; Obata, Y.; Sudo, K.; Kinoshita, M.; Naito, Y.; Sawa, T., Changes in EEG frequency characteristics during sevoflurane general anesthesia: feature extraction by variational mode decomposition. *J Clin Monit Comput* **2023**, *37*, (5), 1179-92.
2. Obata, Y.; Yamada, T.; Akiyama, K.; Sawa, T., Time-trend analysis of the center frequency of the intrinsic mode function from the Hilbert-Huang transform of electroencephalography during general anesthesia: a retrospective observational study. *BMC Anesthesiol* **2023**, *23*, (1), 125.
3. Purdon, P. L.; Sampson, A.; Pavone, K. J.; Brown, E. N., Clinical electroencephalography for anesthesiologists: part I: background and basic signatures. *Anesthesiology* **2015**, *123*, (4), 937-60.
4. Supp, G. G.; Siegel, M.; Hipp, J. F.; Engel, A. K., Cortical hypersynchrony predicts breakdown of sensory processing during loss of consciousness. *Curr Biol* **2011**, *21*, (23), 1988-93.

5. Ching, S.; Cimenser, A.; Purdon, P. L.; Brown, E. N.; Kopell, N. J., Thalamocortical model for a propofol-induced alpha-rhythm associated with loss of consciousness. *Proc Natl Acad Sci U S A* **2010**, *107*, (52), 22665-70.
6. Flores, F. J.; Hartnack, K. E.; Fath, A. B.; Kim, S. E.; Wilson, M. A.; Brown, E. N.; Purdon, P. L., Thalamocortical synchronization during induction and emergence from propofol-induced unconsciousness. *Proc Natl Acad Sci U S A* **2017**, *114*, (32), E6660-E6668.
7. Roche, D.; Mahon, P., Depth of Anesthesia Monitoring. *Anesthesiol Clin* **2021**, *39*, (3), 477-492.
8. Brook, K.; Agarwala, A. V.; Li, F.; Purdon, P. L., Depth of anesthesia monitoring: an argument for its use for patient safety. *Curr Opin Anaesthesiol* **2024**, *37*, (6), 689-696.
9. Brook, K.; Ferraton, M.; Dreher, L.; Lambert, D. H.; Feldman, J. M.; Connor, C. W., Electroencephalographic Depth-of-Anesthesia Monitoring. *A A Pract* **2025**, *19*, (1), e01895.
10. Nguyen-Ky, T.; Wen, P.; Li, Y.; Malan, M., Measuring the hypnotic depth of anaesthesia based on the EEG signal using combined wavelet transform, eigenvector and normalisation techniques. *Comput Biol Med* **2012**, *42*, (6), 680-91.
11. Huang, N. E.; Shen, Z.; Long, S. R.; Wu, M. C.; Shih, H. H.; Zheng, Q.; Yen, N.-C.; Tung, C. C.; Liu, H. H., The empirical mode decomposition and the Hilbert spectrum for nonlinear and non-stationary time series analysis. *Proceedings: Mathematical, Physical and Engineering Sciences* **1998**, *454*, (1971), 903-5.
12. Dragomiretskiy, K.; Zosso, D., Variational mode decomposition. *IEEE Transactions on Signal Processing* **2014**, *62*, (3), 531-4.
13. Gilles, J., Empirical wavelet transform. *IEEE Trans Signal Process* **2013**, *61*, (16), 3999 - 4010.
14. Yamochi, S.; Yamada, T.; Obata, Y.; Sudo, K.; Kinoshita, M.; Akiyama, K.; Sawa, T., Wavelet transform-based mode decomposition for EEG signals under general anesthesia. *PeerJ* **2024**, *12*, e18518.
15. D'ARCY, J. Introducing SSA for Time Series Decomposition. <https://www.kaggle.com/code/jdarcy/introducing-ssa-for-time-series-decomposition> (Dec 12, 2025),
16. Singular spectrum analysis. [https://en.wikipedia.org/wiki/Singular\\_spectrum\\_analysis](https://en.wikipedia.org/wiki/Singular_spectrum_analysis) (Dec 12, 2025),
17. scikit-learn. Machine Learning in Python. <https://scikit-learn.org/stable/> (Dec 13, 20205),
18. Kortelainen, J.; Vayrynen, E., Assessing EEG slow wave activity during anesthesia using Hilbert-Huang Transform. *Annu Int Conf IEEE Eng Med Biol Soc* **2015**, *2015*, 117-20.
19. Liu, Q.; Ma, L.; Fan, S. Z.; Abbod, M. F.; Ai, Q.; Chen, K.; Shieh, J. S., Frontal EEG temporal and spectral dynamics similarity analysis between propofol and desflurane induced anesthesia using Hilbert-Huang transform. *Biomed Res Int* **2018**, *2018*, 4939480.
20. Li, X.; Li, D.; Liang, Z.; Voss, L. J.; Sleight, J. W., Analysis of depth of anesthesia with Hilbert-Huang spectral entropy. *Clin Neurophysiol* **2008**, *119*, (11), 2465-75.
21. Shalhaf, R.; Behnam, H.; Sleight, J. W.; Voss, L. J., Using the Hilbert-Huang transform to measure the electroencephalographic effect of propofol. *Physiol Meas* **2012**, *33*, (2), 271-85.
22. Hayase, K.; Kainuma, A.; Akiyama, K.; Kinoshita, M.; Shibasaki, M.; Sawa, T., Poincare plot area of gamma-band EEG as a measure of emergence from inhalational general anesthesia. *Front Physiol* **2021**, *12*, 627088.
23. Statsmodels. <https://www.statsmodels.org/stable/index.html> (Dec 13, 2025),
24. Sawa, T.; Yamada, T.; Obata, Y., Power spectrum and spectrogram of EEG analysis during general anesthesia: Python-based computer programming analysis. *J Clin Monit Comput* **2022**, *36*, (3), 609-1.
25. Hassani, H. A Brief Introduction to Singular Spectrum Analysis. [https://ssa.cf.ac.uk/ssa2010/a\\_brief\\_introduction\\_to\\_ssa.pdf](https://ssa.cf.ac.uk/ssa2010/a_brief_introduction_to_ssa.pdf) (Dec 13, 2025),
26. Sleight, J. W., Depth of anesthesia: perhaps the patient isn't a submarine. *Anesthesiology* **2011**, *115*, (6), 1149-50.

**Disclaimer/Publisher's Note:** The statements, opinions and data contained in all publications are solely those of the individual author(s) and contributor(s) and not of MDPI and/or the editor(s). MDPI and/or the editor(s) disclaim responsibility for any injury to people or property resulting from any ideas, methods, instructions or products referred to in the content.